Molecular Crystals and Liquid Crystals Science and Technology. Section A. Molecular Crystals and Liquid Crystals

Publication details, including instructions for authors and subscription information:
http://www.tandfonline.com/loi/gmcl19

Orientational Transition and Defect Formation in the Electroconvective State of MBBA

K. S. Krishnamurthy [a] & R. Balakrishnan [a]

[a] Faculty of Electrical and Mechanical Engineering, College of Military Engineering, Pune, 411031, India

Version of record first published: 23 Sep 2006.

To cite this article: K. S. Krishnamurthy & R. Balakrishnan (1995): Orientational Transition and Defect Formation in the Electroconvective State of MBBA, Molecular Crystals and Liquid Crystals Science and Technology. Section A. Molecular Crystals and Liquid Crystals, 264:1, 67-88

To link to this article: http://dx.doi.org/10.1080/10587259508037303

Mol. Cryst. Liq. Cryst., 1995, Vol. 264, pp. 67–88
Reprints available directly from the publisher
Photocopying permitted by license only

Orientational Transition and Defect Formation in the Electroconvective State of MBBA

K. S. KRISHNAMURTHY and R. BALAKRISHNAN

Faculty of Electrical and Mechanical Engineering, College of Military Engineering, Pune 411031, India

(Received November 18, 1993; in final form July 18, 1994)

We have studied the electroconvective behaviour of MBBA, with initial homeotropic boundary conditions, employing a.c. fields acting transversely to the line of sight. Two major types of convective structure occur. They may be described as the distorted-homeotropic (V_D) and distorted-planar (H_D) states. The first bifurcation is to the V_D state and takes place at a threshold voltage which varies parabolically with the electrode-separation. The second bifurcation corresponds to V_D-H_D transformation occurring close to turbulence. The H_D structure, once nucleated, propagates in a highly organized and coherently winding manner so that an array of + 1 linear defects form at the axes of circulation. The growth speed of H_D front is strongly voltage dependent. Field induced undulatory structures develop along the V-H interface below the threshold of electroconvection.

Keywords: Electroconvection, orientational transition, nematic MBBA, defect formation

INTRODUCTION

Freedericksz and Zolina[1] were the first to report of electrohydrodynamic effects in initially homeotropic nematic films driven by transverse fields. In particular, they noted that, on a sudden removal of the field, the fluid relaxing from the turbulent state assumed a schlieren-like, metastable texture. Several years later, while investigating the microstructural changes in MBBA under a varying electric field, Chang[2] examined this texture in some detail and suggested that it could be due to point singularities. Recently, while making a careful study of these defects, which now appear to be linear defects rather than point singularities, we came upon a fascinating new type of electroconvective propagation responsible for their formation. The propagation itself was transient, being characteristic of a heterogeneous transition between the distorted-homeotropic state (V_D), stable at lower voltages, and the distorted-planar state (H_D), forming just prior to turbulence. In a recent communication[3] we have given a brief account of our observations. Detailed characteristics of the V_D and H_D states, and the kinetic aspects of the transformation between them, are discussed here.

EXPERIMENTAL

The liquid crystal (MBBA) investigated was an Eastman Kodak chemical (Cat. No. 11246). It was an old sample kept refrigerated at 5°C prior to use. When purchased, its

electrical conductivity σ was 1.7×10^{-10} S cm^{-1} at 25 °C and the clearing temperature T_C, 45°C. At the time of this study, current-voltage measurements on magnetically aligned samples kept at 25°C showed $\sigma_{\parallel} = 7.7 \times 10^{-9}$ S cm^{-1} and $\sigma_{\perp} = 5.1 \times 10^{-9}$ S cm^{-1}. Also the T_c value was found to have dropped to 37°C. These changes in σ and T_C are not surprising. In the presence of air and moisture, MBBA is known to undergo a gradual hydrolysis and form *p*-anisaldehyde and *p*-*n*-butylaniline.[4,5] These intrinsically non ionic impurities affect the degree of association of the ions in the liquid so that σ is elevated.[4] Further, these impurities lower T_C at the rate of ca. 8°C for every 1% concentration of either impurity (see Figure 1, Reference 5). These earlier findings were found applicable also to our sample: Gas chromatography showed it to be 97.5% pure, and to contain two impurities together amounting to 2.5% concentration. Further, its

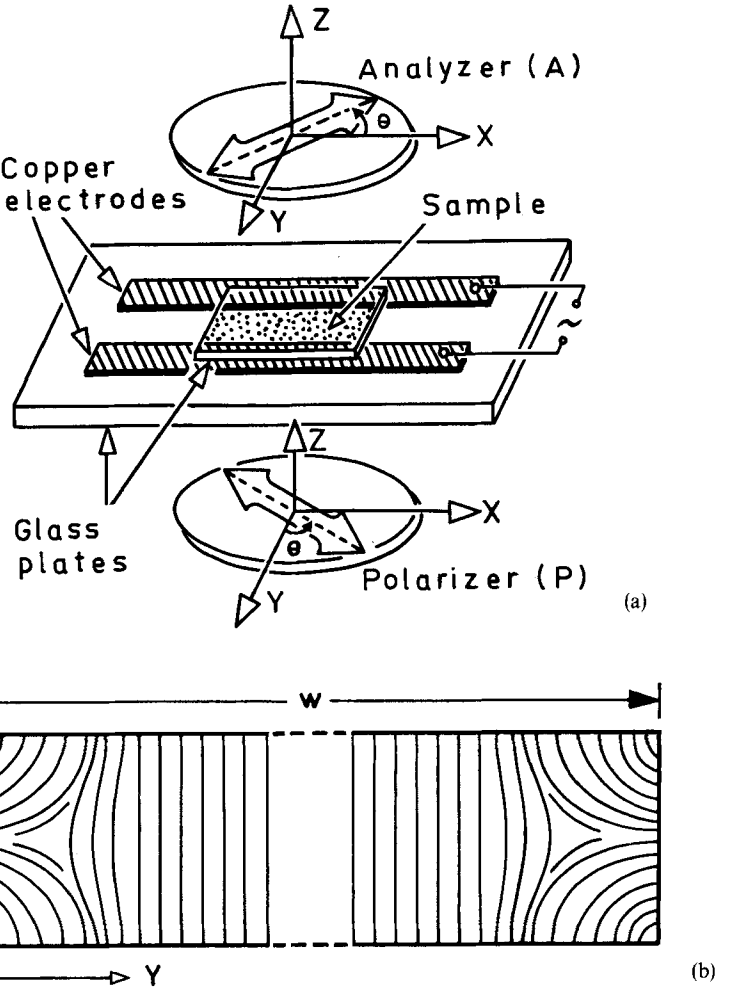

FIGURE 1 (a) Experimental arrangement for observing the electroconvective effects. (b) The initial director field.

infrared spectrum showed two weak absorptions at 3370 cm^{-1} and 3442 cm^{-1}, attributable to the symmetric and asymmetric stretching modes of the NH_2 group in *p-n*-butylaniline. But for these absorptions, the entire spectrum was identical to that of pure MBBA.[6]

Figure 1a shows the experimental geometry. The sample thickness d was 75 ± 5 μm and length l, ~ 1.5 cm; the width w, or the electrode separation, was varied in the range 300 – 1400 μm. The field frequency was 50 Hz. The observations were made on samples maintained at 30°C (unless stated otherwise), along Z, in transmitted light, using a Leitz microscope. Interference effects were studied both in mercury green light and in unfiltered mercury radiation from a commercial discharge source. With the latter, adequate colour separation (not obtainable with white light at higher levels of alignment distortion) was possible and also the colour sequence was similar to that of Newton's scale.[7] The positions of crossed polarizer (P) and analyzer (A) are specified in the text by the angle made by the transmission axis of P with the Y direction. Thus, the configuration P along Y and A along X defines the '0° position'. In Figure 1a, P and A are in the 45° position.

The initial director configuration (Figure 1b) was obtained naturally using chemically clean microscope glass slides for cell fabrication. The sample was introduced into the cell from an end using capillarity. The initial flow induced alignment was homogeneous (H), along X. Very soon, $-1/2$ disclinations formed near the electrode edges as was evident from the characteristic parallel birefringence bands observed in the region, and also the way these fringes shifted with changes in path difference due to a tilting compensator. Beyond the disclination lines, homeotropic (V) zones appeared spontaneously. The V-H boundaries parallel to the electrodes moved inward and merged in the central region in some 15 minutes. With this the initial H zone completely disappeared. The alignment so obtained was indefinitely stable in the absence of any external stress. No special surface treatment was needed to achieve this alignment since its occurrence with untreated plates was very common. However, for comparison a few experiments were performed in which the cell plates had been treated with a 5% solution of cetyl trimethyl ammonium bromide in chloroform; the results obtained were the same as in the earlier case with untreated plates.

RESULTS AND DISCUSSION

Distortion Patterns in the V_D State

Under a progressively increasing a.c. field, the fluid bifurcates at first to the V_D state at a sharply defined and reversible threshold voltage V_{th}. The corresponding optical pattern, unlike the texture of Williams domains in sandwich cells,[8] is spatially homogeneous and nonpropagative. For the 45° setting of crossed polarizers, it consists of a linear array of elliptical birefringent zones appearing evenly spaced along X, against a dark background (Figure 2a). At the centre C of each zone where the distortion originates the path retardation is maximum and the order of interference colours decreases outwards (Figure 2b). We shall for convenience, refer to the region

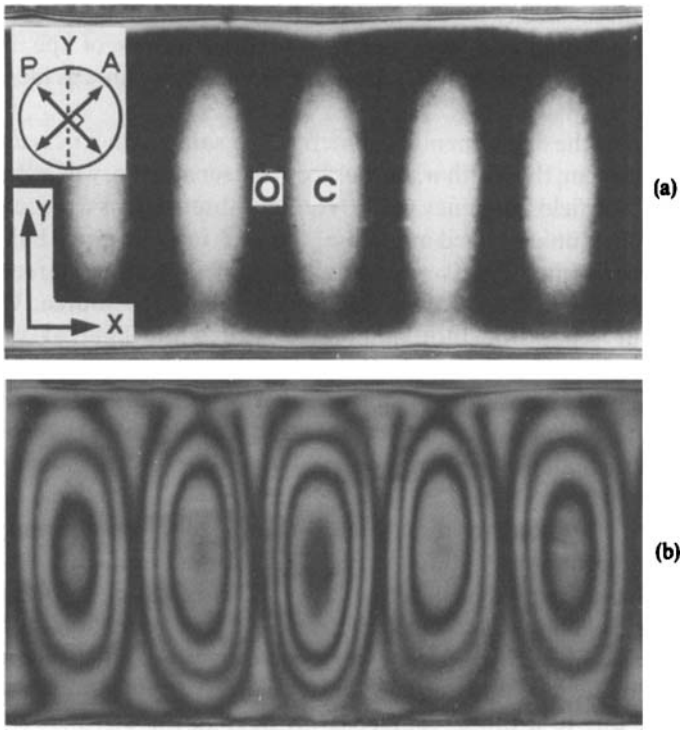

FIGURE 2 Near-threshold textures of the distorted homeotropic state V_D. (a) Pattern of first order white elliptical fringes with parallel bands at the top and bottom edges due to $-1/2$ wedge defects. (b) Interference colours at 1.08 V_{th}. See Colour Plate I.

around each centre C as a 'domain', and treat it differently from the 'convective cell' for reasons to follow later.

Some of the patterns of the V_D state have been reported earlier.[1-3,9] Figure 3, which includes a few of these, shows a systematic development of distortion with voltage. As may be seen in Figure 3 (b, d, f, h), for crossed polarizers in the 0° position, the central region of the domains is dark (or nearly so), showing that the director deviations there are confined to either the XY or YZ plane. That the latter is the case is revealed by the nature of light transmission when using a single polarizer (either P or A in Figure 1a). When the polarizer is set along Y, light travels as an extraordinary wave and gets considerably defocussed in the interdomain regions to produce a series of virtual focal lines periodic in X (see the V_D region in Figure 8a). This effect is absent for the light polarized along X and travelling as an ordinary beam. Hence the director deviations $\theta(z)$ in the sample midregion ($y = w/2, z = d/2$) are of the twist type and periodic in X. The domain periodicity, or the distance between alternate domain centres, is not very sensitive to interelectrode separation, and is equal to about six times the sample thickness as in the case of the domains in freely suspended nematic films.[10] Excepting a few closed fringes near the centre C, the others generally involve molecular deviations out of the YZ plane, as could be inferred by the appearance of birefringence fringes near

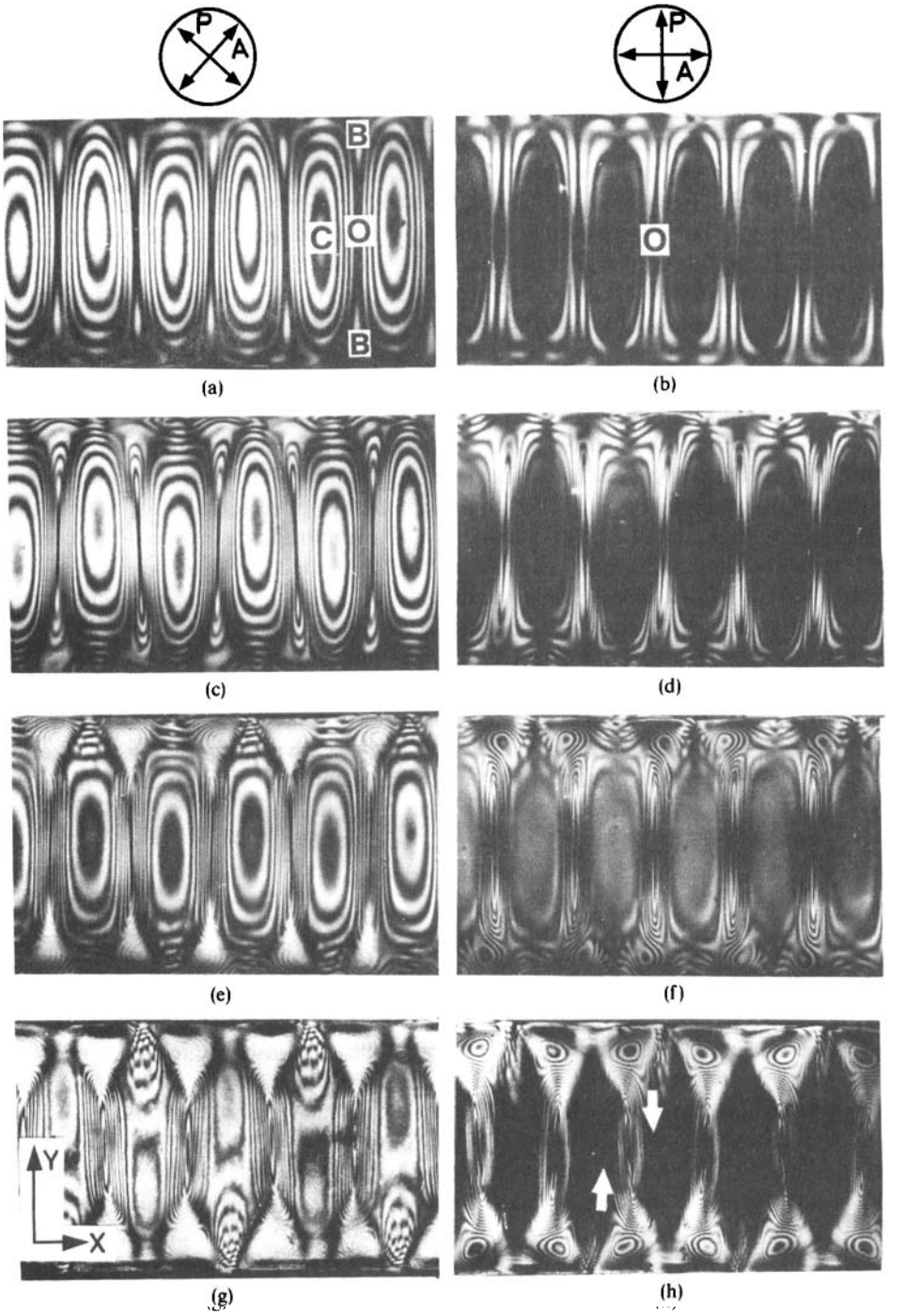

FIGURE 3 Textural changes in the V_D state with progressive rise in voltage. 720 μm wide sample. Crossed polarizers set diagonally for (a, c, e, g) and along X and Y for (b, d, f, h). (a, b) 62 V_{rms}; (c, d) 70 V_{rms}; (e, f) 74 V_{rms}; and (g, h) 76 V_{rms}. 50 Hz.

the domain boundaries along Y, when using crossed polarizers in the 0° position (Figure 3b). In the central zone O of the interdomain boundary, the director orientation remains undisturbed at all voltages so long as the pattern is static. This is indicated by the darkness seen at O for all orientations of crossed polarizers (Figures 3a–h). The director configuration corresponding to these observations is provided in Reference 3.

When the voltage reaches about $1.3\,V_{th}$, a secondary instability appears in the B regions of the interdomain boundary, on either side of O. It is marked by the evolution there of new systems of birefringence fringes having the following characteristics: The fringe-order in a given system is the highest at the centre and the pattern-geometry is indicative of the flow direction (see the arrows in Figure 3h). Unlike the fringes around C, those of the B zones are clearly visible for the 0° position of crossed polarizers (Figures 3f and 3h); their visibility is poor for the diagonal position (Figures 3e and 3g). Further, the B zones turn partially dark when P and A are parallel, set at $\pm 45°$ to Y, and completely dark when the polarizers are aligned as in Figures 4a and 4b. The darkness is not much affected by a further rise in voltage (to, say, $1.4\,V_{th}$); but the number of birefringence bands at B increases markedly with it. These observations are correlated with the director tilt $\theta(z)$ and twist $\phi(z)$ (Figure 4c). A possibility is that, effectively, ϕ changes gradually from $+30°$ near the entrance ($z = 0$) to $-30°$ near the exit ($z = d$), through 0° at the centre ($z = d/2$), as illustrated in Figure 4c. The resulting optical activity, which was earlier[3] thought to be of opposite sense for adjacent B zones along X, has to be uniformly left- or right-handed for all the B zones, since otherwise the same configuration of polarizers as in Figure 4a cannot result in blocking of light for all the B zones. As for the tilt $\theta(z)$, it increases from zero at either of the glass plates to a maximum at the centre ($z = d/2$); its range of variation or the effective path retardation diminishes radially outwards in a given B zone. Unlike ϕ, θ is strongly voltage dependent. The nature of coupling between the director alignment and hydrodynamic flows responsible for these and other high voltage textural features of the V_D fluid remains to be understood.

V_D Threshold as a Function of Interelectrode Distance

The threshold voltage V_{th} of the V_D instability is significantly affected by the electrode separation w. This has been noted earlier, but no detailed measurements have been published so far. In this study, we take V_{th} as the voltage at which the first order interference gray colour is observed. The value so determined is evidently an overestimate as it corresponds to a finite distortion. The actual optical threshold as deduced from the voltage-phase retardation plots is about 1.3% lower than V_{th}. We find the dependence of V_{th} on w to be nonlinear (Figure 5). For freely suspended nematic films of MBBA Faetti *et al.*[10] find V_{th} to scale linearly with w and explain this observation theoretically on the basis of the Carr–Helfrich model. However, their measurements are confined to a range of w from 350 to 600 μm, and the nonlinearity shown in Figure 5 is not so pronounced as to reveal itself for such a limited range. Secondly, the experimental boundary conditions for freely suspended films are quite different from those obtaining here so that the results of the two experiments could vary. For example, unlike here, in suspended nematic films, the sample thickness is non-uniform, the

hydrodynamic currents exist at the free surfaces rather than in the midplane, and space charges build up near the free surfaces. Interestingly, for suspended smectic films of uniform thickness, the onset voltage of electroconvection measured over a wide range of electrode separation shows a nonlinear behaviour as in Figure 5.[11] For wider samples, it is possible that the decreased effect of lateral boundaries would result in lower thresholds of instability originating in the midregion.

Hydrodynamic Flow in the V_D State

A correlated motion of dust particles in the V_D fluid becomes readily noticeable at higher voltages ($> 1.2\ V_{th}$). It reveals a flow pattern consisting of a series of vortex cells

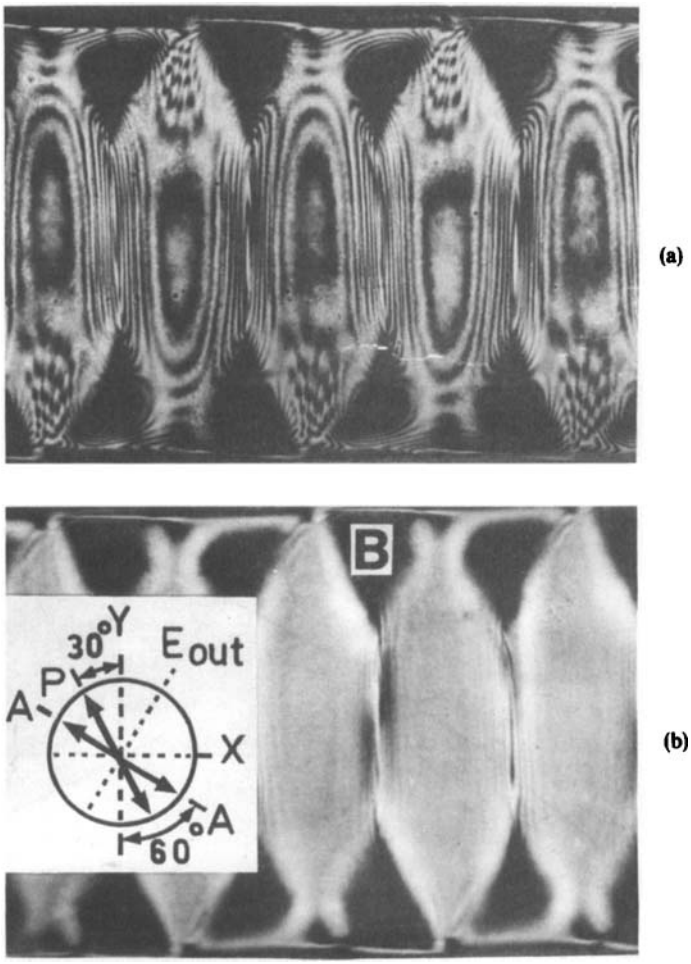

FIGURE 4 Localized optical activity in the V_D fluid. The dark areas B in (a) and (b) arise due to rotation of the incident electric vector (along the polarizer P) to the position marked E_{out}. analyzer A is at 90° to E_{out}. (c) Schematic representation of possible director reorientations along the axes B_1B_3 and B_2B_4 of two adjacent B zones along X; the diagram also applies to two opposite B zones along Y.

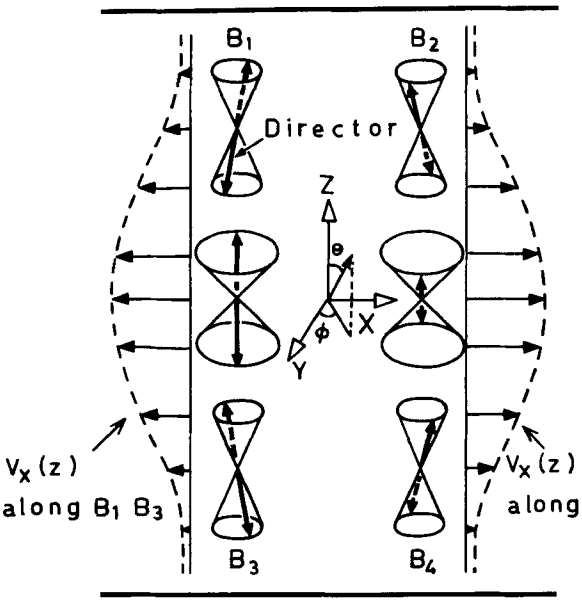

(c)

FIGURE 4 *(Continued)*

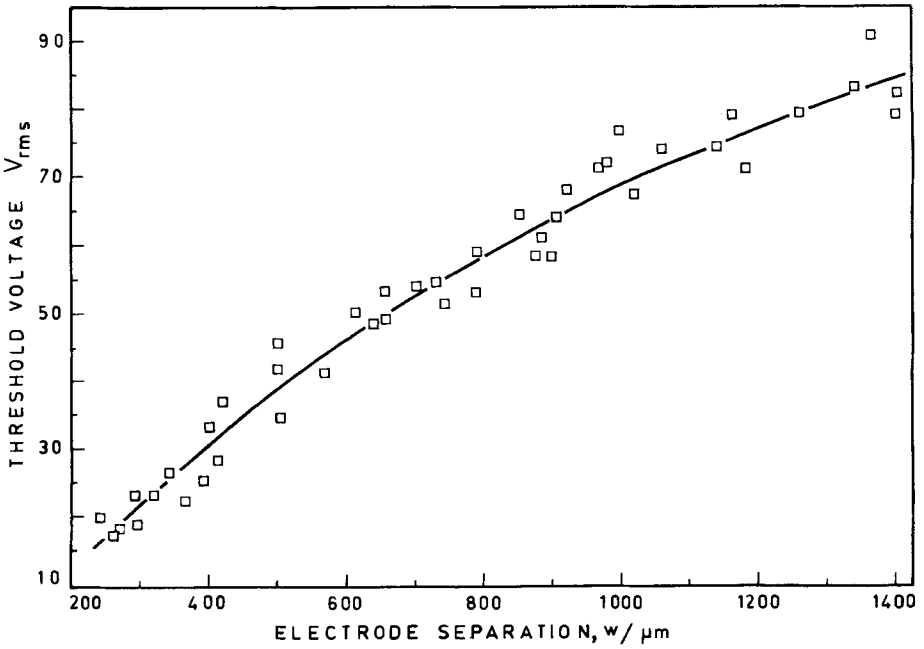

FIGURE 5 Threshold voltage of the distorted homeotropic state as a function of interelectrode distance.

of alternating vorticity along X. The streamlines are ellipses lying in the XY plane with their major axes along Y and centres at point O (Figure 3a) where the original alignment is undisturbed. In other words, a given flow cell is not entirely located within the space occupied by a domain, but is divided between adjacent domains. Along a given flow line, the particle speed varies continuously being maximum in the sample midregion and minimum closest to the electrodes. Further, for a given vortex, the flow is swiftest at points such as C in Figure 3a where the alignment distortion is maximum. It is noteworthy that along a streamline the molecular tilt varies here continuously unlike in sandwich cells for Williams rolls.[12] It is also significant that the vortex lines lie in the XY plane: In sandwich cells, the fluid revolves in planes defined by the initial director and the field, and around regions of maximum director deflection. A corresponding behaviour for the transverse geometry requires the vortex flows to occur in the YZ (rather than XY) plane. In that case, the tracer particles viewed along Z should appear to traverse back and forth along Y. Indeed such a motion has previously been reported[9] for samples with magnetic field induced, uniformly homeotropic initial alignment involving no line singularity as in Figure 1b. The nature of convective flows is of course determined by the distribution of conduction induced space charges. If we consider the alignment distortions to be purely of the twist-bend type, dependent only on the X and Z coordinates, the charge separation would be expected to be as in Figure 6. This could produce cellular flows either in the XY or the YZ plane. In the former case, two vortex rows should form, one above the central XY plane and the other below it. Further, the vorticity should be opposite in adjacent flow cells of a given row (along X) as well as in the pair of flow cells around a given axis (along Z). In fact, for freely suspended nematic films, as shown by Faetti *et al.*[10] the model in Figure 6 applies

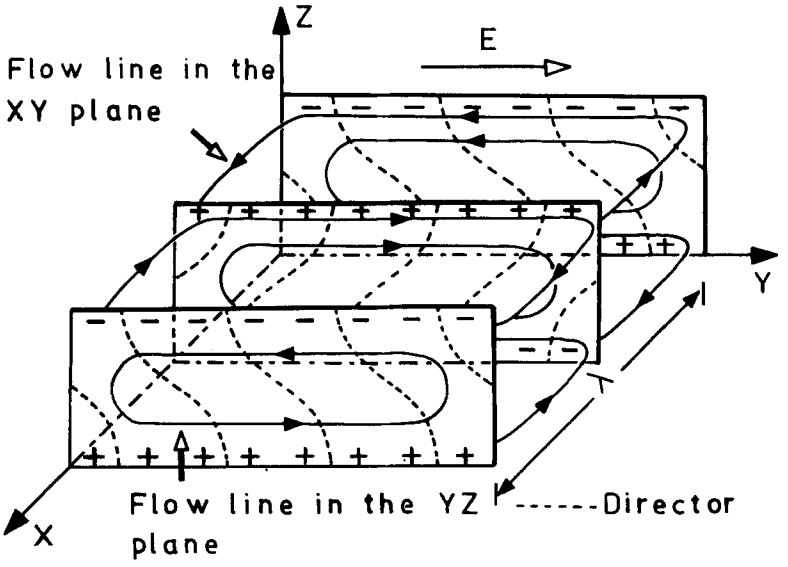

FIGURE 6 Schematic diagram illustrating the space charge build up in the film under a transverse electric field, assuming only twist-bend type distortions. The observed flow field rules out this type of charge focussing in the present study.

and the flows occur in the XY plane as expected. However, under the boundary conditions on flow velocity used here, only a single roll is observed around a given axis and the dust particles at different depths in the fluid rotate in the same sense. Clearly, the model in Figure 6 is not applicable to the present case. Here the space charges which are of the same sign in a given YZ plane accumulate in the midregion (with respect to Z) so that positive and negative layers occur alternately and periodically along X. The alignment distortion causing this charge build up remains to be understood. It is evidently more complex than indicated in Figure 6 and is essentially three dimensional as might be expected from Figure 3.

The fluid velocity is a function of all the co-ordinates x, y and z. We determined the average value $\bar{v}_y$ in the central region of the cell and along the flow line corresponding to the highest speed in a given vortex. For this purpose, we measured the time of traverse of dust particles of size 5–10 μm through a distance of 146 μm along Y in the midregion. The sample widths varied between 580 and 750 μm. Figure 7 shows the data for $\bar{v}_y$ plotted against the dimensionless stress (or control) parameter $\varepsilon = (V/V_{th})^2 - 1$. As may be seen in the inset, $\bar{v}_y$ varies as $\varepsilon^{0.77}$ Previous experiments on flow velocity concern MBBA samples aligned homogeneously in the rest state and studied either in the longitudinal[13] or transverse geometry.[14,15] In References 13 and 14, the data show a linear variation of $\bar{v}_y$ in ε. However, the variation found in Reference 15 is consistent

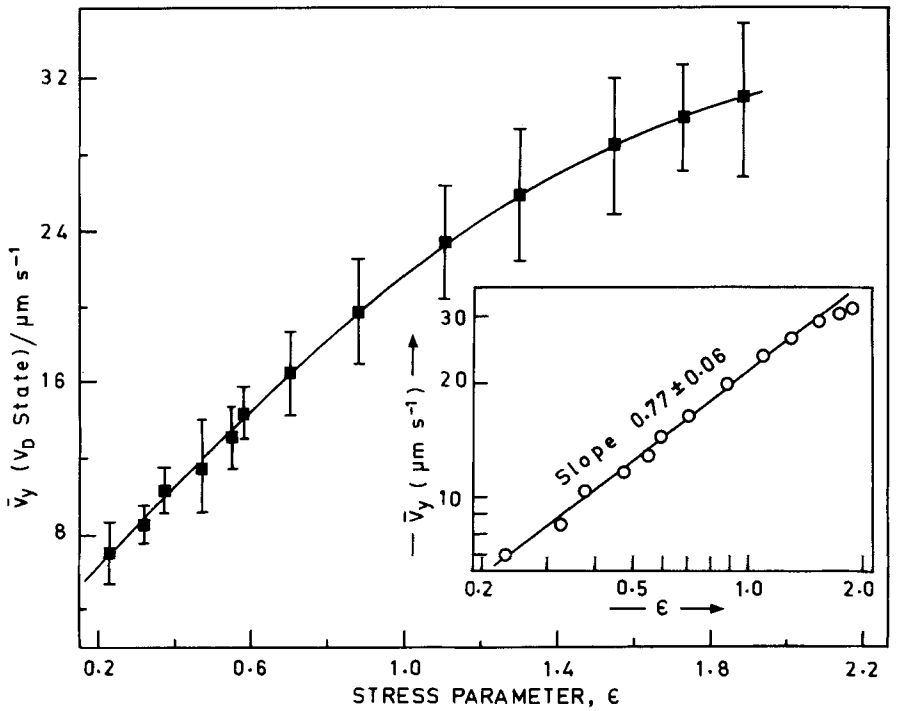

FIGURE 7 Average vortex velocity $\bar{v}_y$ for the V_D state as a function of the stress parameter $\varepsilon = (V/V_{th})^2 - 1$.

with that shown in Figure 7 here. Theoretically the flow velocity is expected to vary as E^2/η where E is the field strength and η the effective viscosity coefficient.[16] At elevated field strengths the value of η may vary because of nonlinear processes, thus affecting the linearity of $\bar{v}_y$ in E^2.

Transition to the H_D State

In a previous report,[3] we have described the nature of transition from the V_D to H_D state. For further characterization of this transition, it is helpful first to review its salient aspects: When the alignment distortion reaches the complexity indicated in Figure 3h ($V = 1.4\,V_{th}$), the V_D state becomes unstable and undergoes a heterogeneous structural change into the distorted planar state. This change lacks a definite threshold and requires nucleation. It originates usually at either of the end free-surfaces in a matter of some 10 minutes after the voltage is raised to about $1.4\,V_{th}$ and its occurrence is accelerated at higher voltages. Figure 8 shows the propagation behaviour of the H_D front. It advances in a coherently winding manner from one end of the sample to the other. Figures 8a–c show how the H_D front developing from the left progressively loops around the third interdomain junction O in a clockwise manner. Figure 8d shows the commencement of circulation around the next junction in an anticlockwise sense. In Figure 8f giving the final H_D texture, periodic sharp (S) and blunt (D) peaks are seen along the electrode edges. These are due to parts of the fluid in contact with the electrodes that do not undergo the reorientational transition into the H_D state. Those fluid parts that are dragged by the invading H_D current during the transition show up as spikes S and the parts that are pushed back by the current appear as humps D. Some of the colourful birefringence patterns of the V_D and H_D states are presented in Figure 9. In Figure 9a, the central elliptical fringes of the V_D domains are replaced by triangle-like fringes in the H_D state. Significantly, as we go outward from the centre of these closed fringes, the colours fall (on Newton's scale) for the elliptical fringes, but rise for the triangular ones. The same feature is observed also for the closed fringes appearing in the B zones, near the electrodes. These observations could be correlated with the predominantly vertical and planar structures of the V_D and H_D fluids, respectively.

Both the convective instabilities V_D and H_D are anisotropic in that they disappear above T_C. The sense of fluid rotation at various points also remains unchanged on passing from the V_D to the H_D state. However, after the transition, the planform of the vortices of flow is strongly tilted with respect to X and Y, unlike in the V_D state. The sign of tilt is opposite for adjacent vortices, and the tilt angle between the major axis of a flow line and the Ydirection is about 20°. If after the transition the voltage applied to the H_D fluid is lowered gradually, this tilt angle decreases, tending to 0° as V_{th} is approached. Obviously the degree of distortion determines the extent of obliquity. It is therefore likely, the anisotropy of elastic coefficients are related with this nonlinear feature as in the case of the 'squint' effect in Williams rolls.[17]

The speed of traverse of the H_D front around a domain junction varies continuously. In the central region of the film, the flow is the swiftest and is directed along $\pm Y$. Near the electrodes, it is along $\pm X$ and is the slowest. We measured the average velocity $\bar{v}_y$ in the central region by timing the advance of the front through an interval of 146 μm. For estimating the forward velocity $\bar{v}_x$ along X, we measured the time of propagation

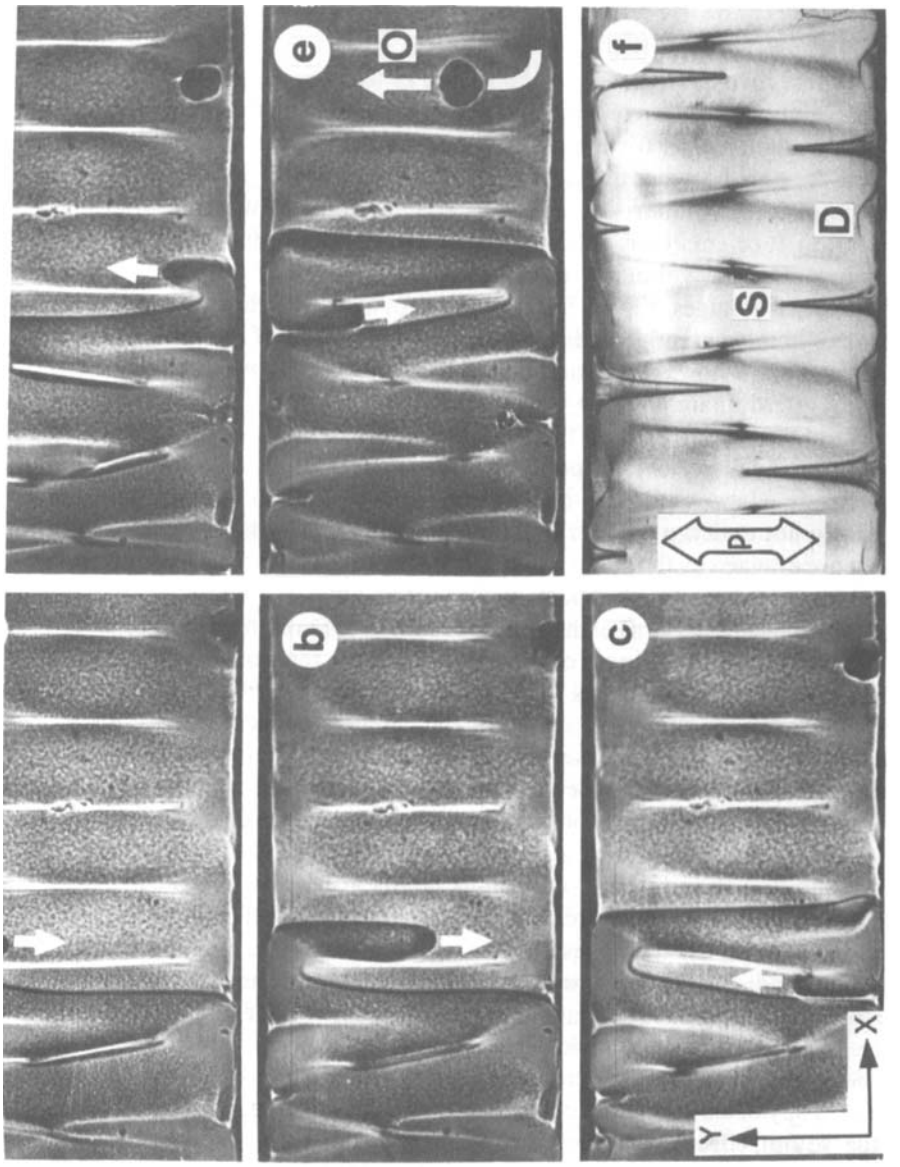

FIGURE 8(a–e) Time evolution of the distorted planar structure H_D from the distorted homeotropic structure V_D showing an organized propagative transition. Microscope focused on bright vertical lines which are the virtual focal lines seen along the interdomain boundaries in the V_D state. The grainy appearance between the focal lines is caused by the Brownian motion in the fluid and is characteristic of the region through which light travels as the extraordinary beam. The dark object revolving around O in (e) is a large, defocused dust particle. Exposure time 1/125 s. (f) H_D texture; microscope focussed on the sample midplane.

through a distance of 1155 μm corresponding to about five successive V_D vortices passed by the front. The H_D transition is associated with a large hysteresis in that the H_D front, once formed, maintains its propagation even on reducing the voltage to less than V_{th}, provided the new voltage is close to it. Thus the H_D flow velocity measurements could be extended to slightly lower values than V_{th}.

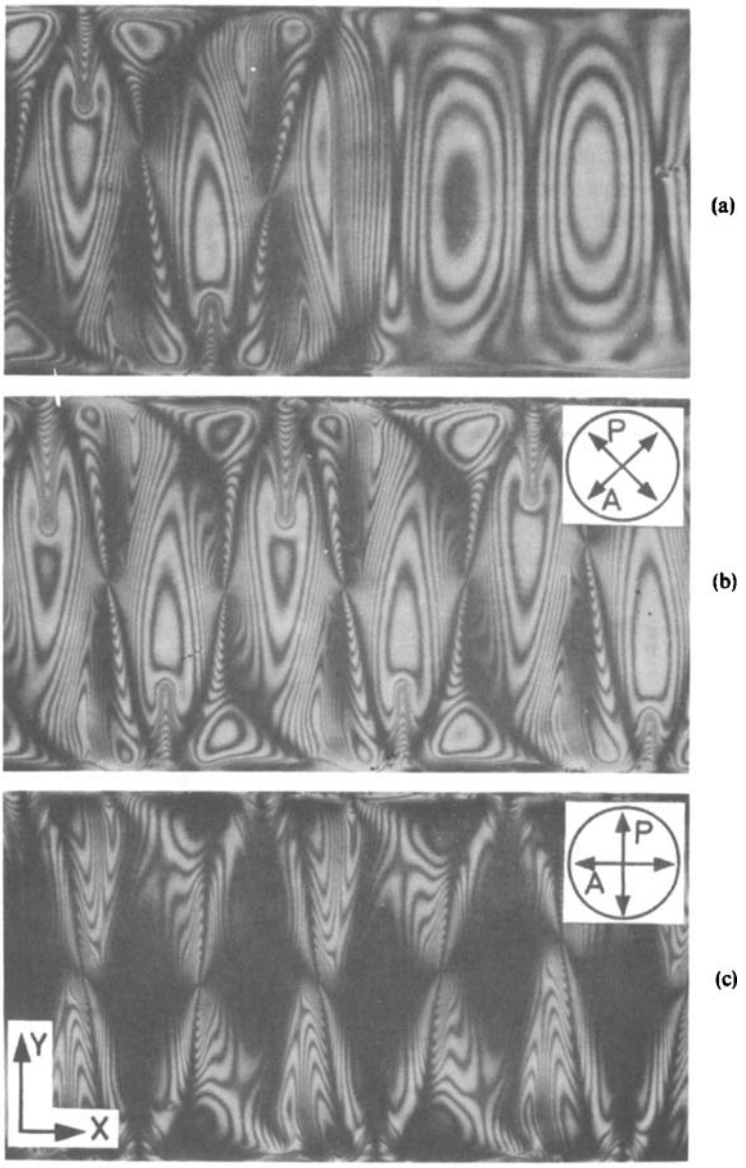

FIGURE 9 Interference colours in the V_D and H_D states recorded at 1.13 V_{th}; 745 μm wide sample. (a) Texture during the V_D-H_D transition. (b, c) Textures of the H_D state. Crossed polarizers in the 45° position for (*a*) and (*b*), and along *X* and *Y* for (c). See Colour Plate II.

Figure 10 shows the voltage variation of $\bar{v}_y$ for a 700 μm wide sample. This nonlinear plot may be regarded as comprising three regions corresponding to different conditions of the H_D front propagation. The first lies below 55 V, which is the V_{th} value for the sample. The data here are obtained by lowering the voltage to less than V_{th} after the H_D nucleation so that the V_D region returns to the rest state and the H_D front propagates into the V state. The second belongs to the range 55–70 V, and in this region, the mode of H_D front circulation is of one type in which always a new front cycle begins only at the end of the previous one. The region above 70 V corresponds to a second mode of H_D propagation in which a new front cycle begins while the earlier one is still in progress. Figure 11 showing $\bar{v}_y$ as a function of electrode gap w, is also in agreement with the dependence of $\bar{v}_y$ on the mode of H_D front advance. The regime of w below the arrow mark in the figure corresponds to the second mode of flow, whereas that beyond the arrow belongs to the first mode. In Figure 12 showing the voltage dependence of $\bar{v}_x$, there is a large scatter of points and no regular trend as in Figures 10 and 11 could be

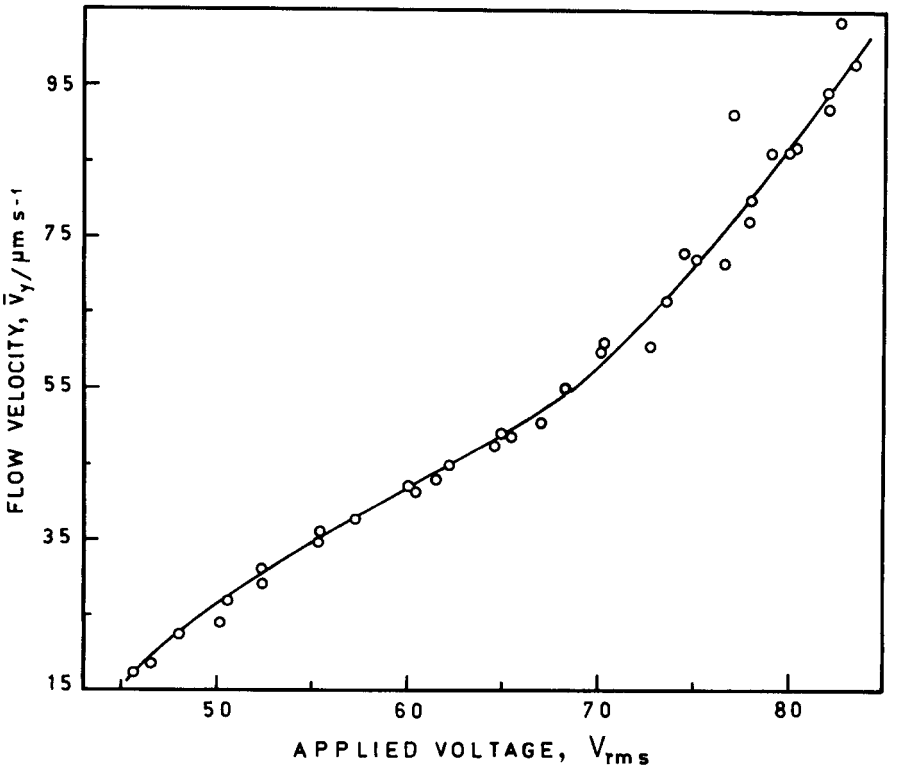

FIGURE 10 Average velocity of advance of the H_D front in the sample midregion as a function of applied voltage. 700 μm wide sample.

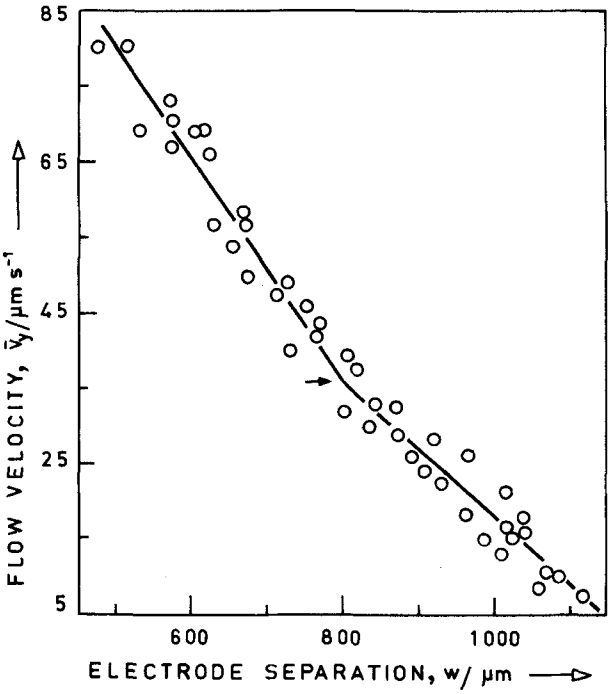

FIGURE 11 Average velocity of advance of the H_D front in the sample midregion as a function of electrode separation. $V_{rms} = 70$ volts.

traced. This is presumably because the time of start of every new cycle near the electrodes is somewhat uncertain. This is especially so for lower voltages for which the horizontal velocities are very low.

Apart from the two main modes of vortex propagation just mentioned, there exists another mode of flow in the voltage region significantly below V_{th}. In this mode, the H_D front propagates as a narrow band, coursing between the electrodes in a regular sinusoidal manner. This type of propagation often terminates with the width of the H_D band becoming ever narrower with the advance. On the other hand, if the voltage is increased to bring the fluid close to the chaotic state, the H_D front breaks up in the central region into islands. Yet, each island circulates along the original path and the modes of circulation are reversible by reducing the voltage appropriately. In any case, voltage variations will not induce the H_D state to transform back to the V_D state. At lower voltages, it transforms directly to the V state, as described later.

Hydrodynamic Flow in the H_D State

We measured the average flow velocity $\bar{v}_y$ in the H_D fluid just as for the V_D fluid, by following the motion of suspended particles. The data in Figure 13 pertain to a sample with $V_{th} = 40\,V_{rms}$. Comparison of Figures 7 and 13 shows that $\bar{v}_y$ is marginally greater in the H_D fluid above $\varepsilon = 0.4$, but becomes markedly greater below this value. Whereas

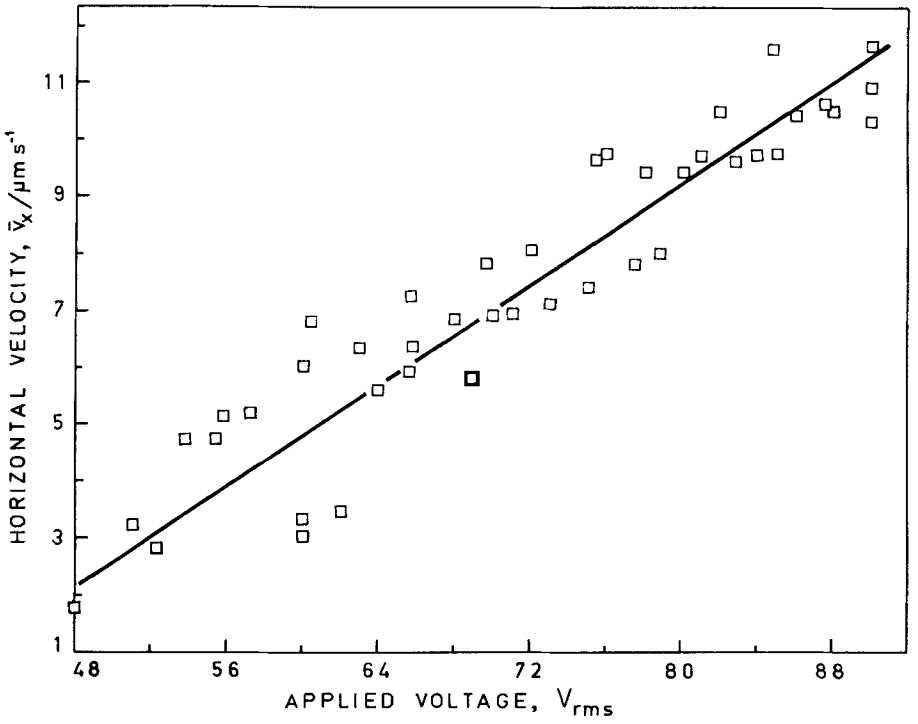

FIGURE 12 Average rate of advance of the H_D front along X as a function of the applied voltage. 700 μm wide sample.

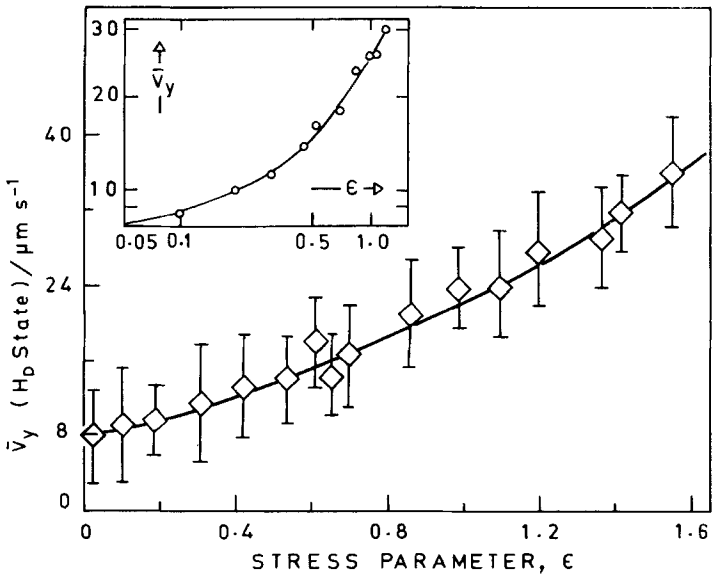

FIGURE 13 Average vortex velocity $\bar{v}_y$ for the H_D state as a function of the stress parameter $\varepsilon = (V/V_{th})^2 - 1$. V_{th} is the threshold for the V_D state.

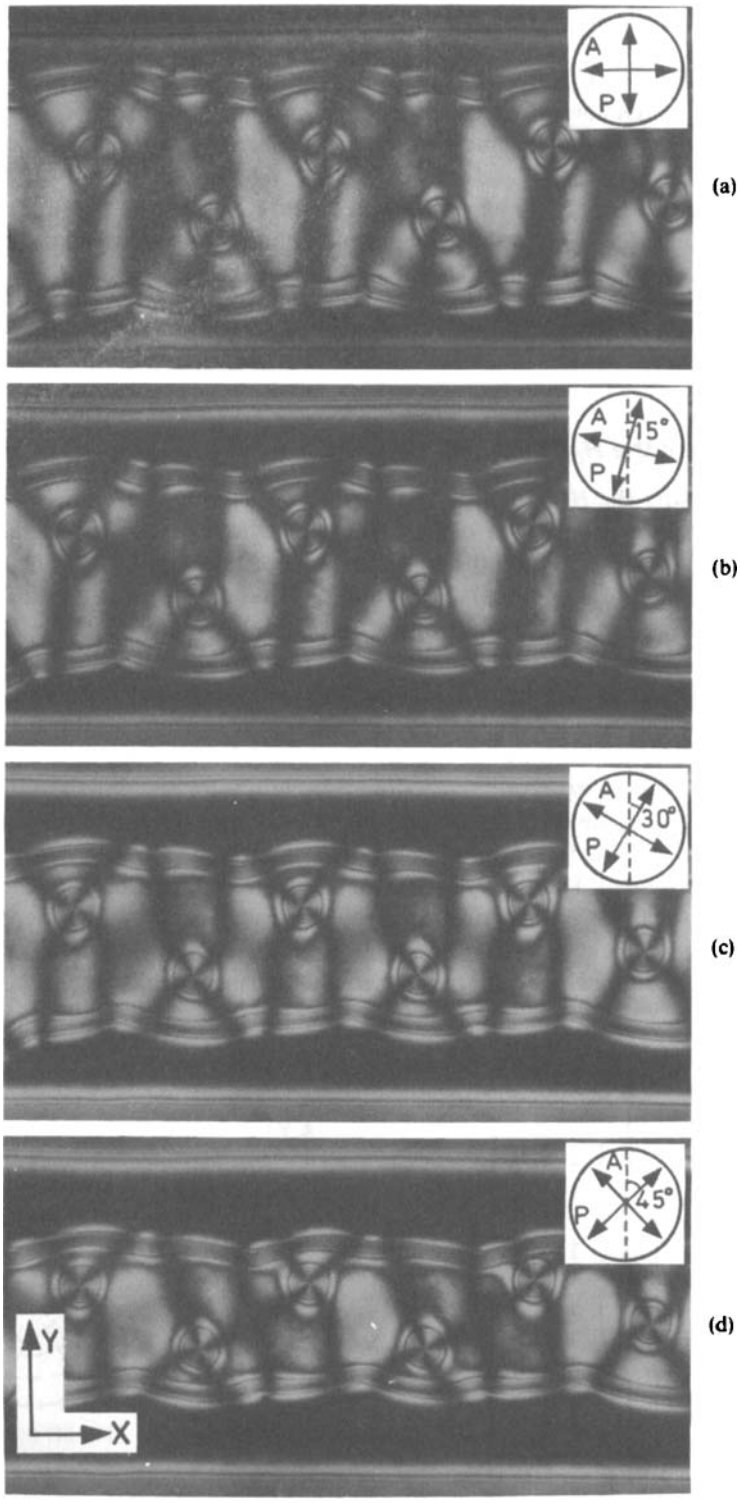

FIGURE 14 Birefringence colours in the degenerate planar structure H to which the H_D structure relaxes in the field-off state. The time photographs show an array of +1 linear defects in the midregion of a collapsing H domain; the dark regions on either side of H belong to the V state. Periodic −1/2 disclinations are located

$\bar{v}_y \to 0$ as $\varepsilon \to 0$ in the V_D state as expected, $\bar{v}_y$ is as high as 8 μm/s even at $\varepsilon = 0$ for the H_D fluid. In fact a well correlated, sustained dust particle motion is discernable in the H_D state down to $\varepsilon = 0$, but this motion is scarcely seen in the V_D fluid below $\varepsilon \approx 0.2$. In general, for the H_D fluid, $\bar{v}_y$ and ε are not related by a power function, unlike in the V_D fluid (see inset, Figure 13). These differences seem to arise from the way ε is defined in Figure 13. Since the V_D-H_D transition has no definite threshold and also since the H_D state is stable at V_{th}, we took V_{th} of the V_D state in defining ε. But the H_D state and the convective flows persist below V_{th} as well. Therefore, ε in Figure 13 may not represent the actual control parameter. Because of the matastability of H_D state below V_{th}, it seems difficult to define a more meaningful ε for this state.

Relaxation of the H_D Structure

The reason why the H_D structure is described as essentially planar is that, when the field maintaining it is turned off, it relaxes to what may be called the degenerate planar state (H),[18] and not the original homeotropic state (V). The H structure, in which the axes of fluid circulation of the precursor state remain as an array of +1 linear defects, is metastable and transforms into the V state gradually. The sequence of events associated with this change is : formation of −1/2 line defects near the electrode-edges, development of V zones between these defects and the central H zone, and an inward advance of the V-H interface parallel to itself causing a collapse and eventual disappearance of the H zone. The fascinating birefringence colours displayed by the H structure and its metastable nature are illustrated in Figure 14. The birefringence colours of the H zone do not show any marked variation during H-V transformation. Nor do the interference fringes formed in the region of +1 defects show any movement. These facts preclude changes in H structure along the Z direction. The H-collapse takes place mainly along $\pm Y$, through twist type reorientations. That the interference fringes seen at the V-H walls in Figure 14 arise from twist type deformations could be inferred from the nature of fringe displacements accompanying

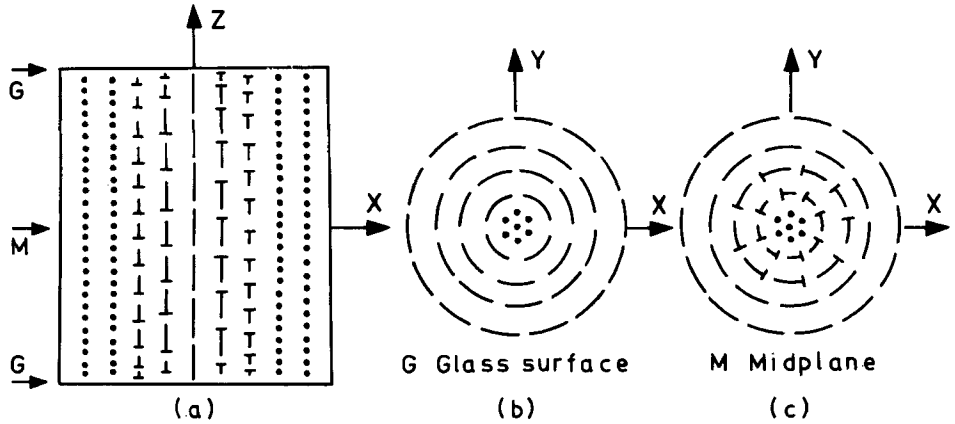

FIGURE 15 Director pattern for the +1 defects in Figure 14.

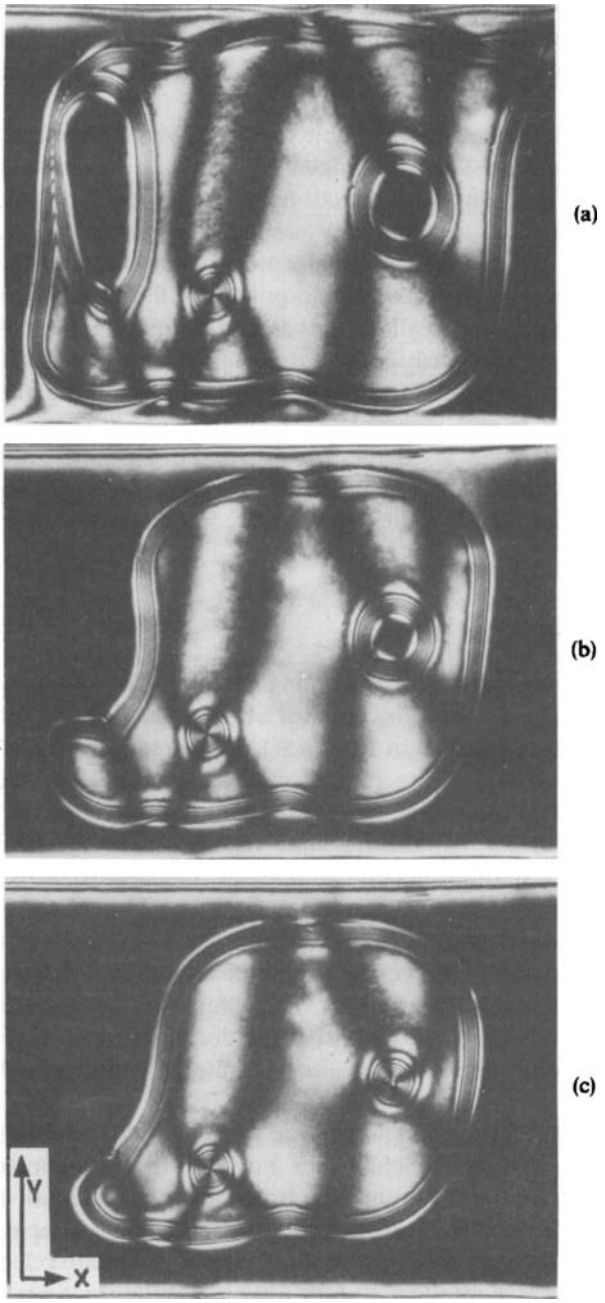

FIGURE 16 Time photographs of a metastable *H* domain within which a homeotropic island collapses two-dimensionally to form a linear defect. Crossed polarizers aligned diagonally.

phase changes produced by a tilting compensator plate. The walls appear slightly wavy due to the formation at regular intervals of $-1/2$ disclinations along these boundaries. The director field corresponding to the texture in Figure 14 is given in Reference 3.

As could be ascertained using a variable compensator, the molecular arrangement around the $+1$ defects is essentially tangential. While at the defect-core the director is normal, in a radially outward direction in the midplane, it tilts progressively about this direction so as to eventually assume a planar configuration. The core is thus nonsingular, but the end points are not. In the plane of the glass surfaces, the director is tangentially disposed around point singularities (Figure 15). Following Saupe,[19] such defects may be called threads ending in singular points. That these are not point defects as previously conjectured may also be inferred from the textures in Figure 16. The texture in Figure 16a is recorded by turning the field off when the V_D-H_D transition is still incomplete. It shows two V islands in a collapsing H domain; in the field on state these were in the V_D state surrounded by the invading H_D front. With time, as seen in Figures 16b and 16c, one of the islands shrinks laterally, to form a line defect, while the other becomes a part of the expanding outer V region.

Undulating Walls Induced Below V_{th}

As earlier noted, during the course of winding advancement of the H_D front, a part of the fluid contiguous to the electrodes remains 'stagnant' and shows itself as alternately sharp and blunt peaks (S and D in Figure 8f). These regions are associated with an interesting aspect concerning the rate of collapse of the H-domains. If after the formation of the H_D state above the V_D threshold, the voltage is decreased to a nonzero value, considerably below V_{th}, the H_D state relaxes to the H state, which in turn collapses laterally in a spatially dependent manner. The inward movement of the V-H boundary is faster in the S region than in the D region. Thus the V-H interface turns undulatory and the wave-amplitude grows with time. The H-zone as a whole appears like a sinusoidal band becoming ever narrower; the regions of $+1$ defects endure till the final stage of disappearance of the H-zone. The differential collapse rate along the V-H wall becomes progressively less pronounced with decreasing voltage (Figure 17). In the field off state, the walls move at an almost uniform rate everywhere, as seen in Figure 14.

The wavy V-H boundaries in Figure 17 are strongly reminescent of the undulatory structures observed earlier by Schell and Porter[20] in a homeotropically aligned sample of 5CB (cyano-pentyl biphenyl) driven by a horizontal a.c. field. There, between crossed polarizers, the surface oriented dark V zone is seen flanked between two electrically reoriented birefringent H zones formed next to the electrodes; the wave pattern appears at the H-V interface and the wave-amplitude increases with the applied voltage as in this study. These observations have been qualitatively explained by envisaging a periodic space charge build up along the H-V boundary. This explanation should equally apply for the wave structures observed here. However, the circumstances leading to this common phenomenon are, as it were, of opposite character: with 5CB, the waves form in the dielectric regime, above the threshold for Freedericksz

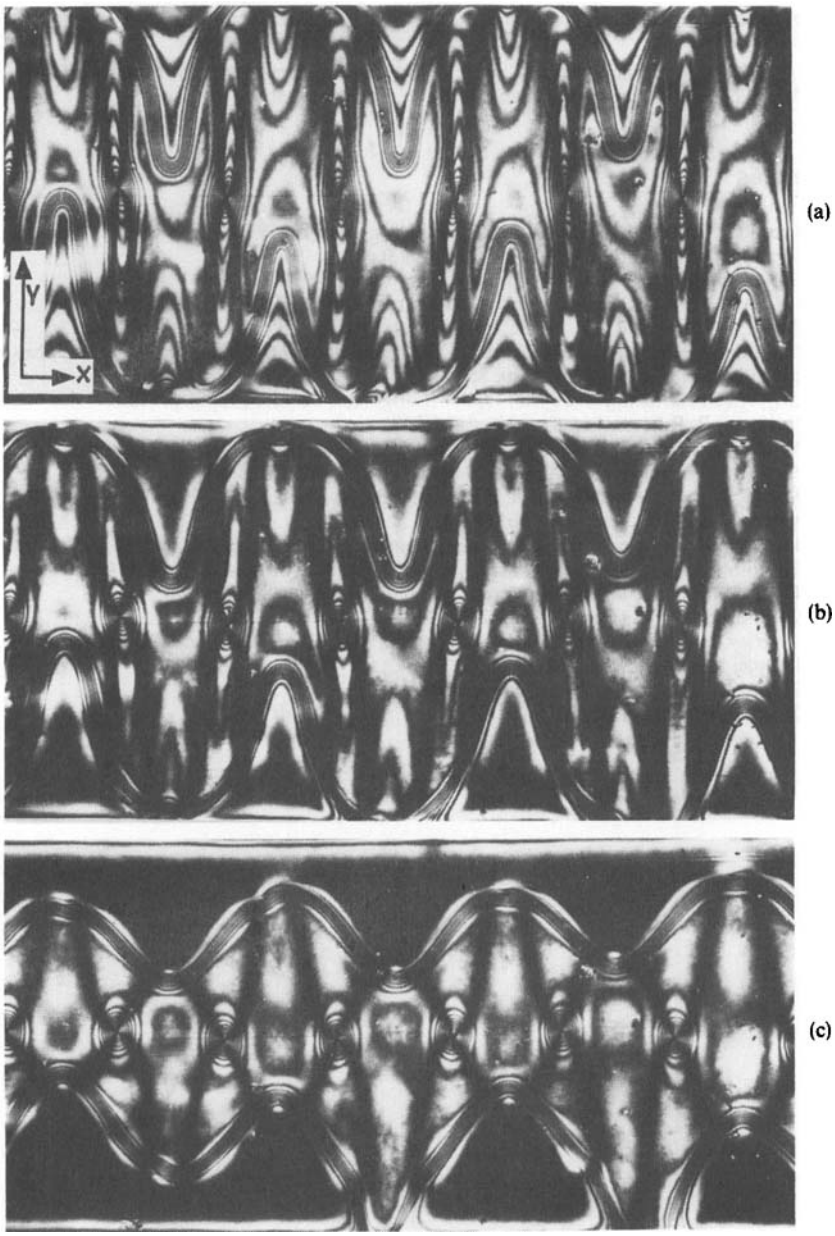

FIGURE 17 Interferograms of a planar H domain obtained after suddenly reducing the voltage from 65 V_{rms} to 40 V_{rms} (a), 40 V_{rms} to 30 V_{rms} (b) and 30 V_{rms} to 20 V_{rms} (c), showing the characteristic undulatory structures at the V-H boundaries and the decreasing wave-amplitude from (a) to (c).

deformation, when the electrically generated torques render the V state unstable: whereas with MBBA, they form in the conduction regime, below the threshold of electroconvection, when the surface generated elastic torques render the H state metastable.

Acknowledgements

We are grateful to the Commandant, College of Military Engineering for the experimental facilities and to Brig . Dr. S. G. Vombatkere for his keen interest in this investigation.

References

1. V. Freedericksz and V. Zolina, *Trans. Faraday Soc.*, **29**, 919 (1933).
2. R. Chang, *Mol. Cryst. Liq. Cryst.*, **44**, 1885 (1973).
3. K. S. Krishnamurthy and R. Balakrishnan, *Liq. Cryst.*, **16**, 413 (1994).
4. L. T. Creagh and A. R. Kmetz, *J. Electron. Mater.*, **1**, 350 (1972).
5. A. Denat, B. Gosse and J. P. Gosse, *Chem. Phys. Lett.*, **18**, 235 (1973).
6. B. J. Bulkin, T. Kennelly and W. B. Lok, *Liquid Crystals and Ordered Fluids II*, J. F. Johnson and R. S, Porter (Plenum, New York, 1974), p. 85
7. P. Gay, An Introduction to Crystal Optics (Longmans, London, 1967), p. 115.
8. A. Joets and R. Ribotta, *Liq. Cryst.*, **5**, 717 (1989).
9. N. V. Madhusudana, P. P. Karat and S. Chandrasekhar, *Current Sci.*, **42**, 147 (1973).
10. S. Faetti, L. Fronzoni and P. A. Rolla, *J. Chem. Phys.*, **79**, 1427 (1983).
11. S. W. Morris, J. R. de Bruyn and A. D. May, *Phys. Rev.*, A**44**, 8146 (1991).
12. P. A. Penz, *Phys. Rev. Lett.*, **24**, 1405 (1970).
13. G. Durand, M. Veyssie, F. Rondelez and L. Leger, *C. R. Acad. Sc.* (Paris), **B 270**, 97 (1970).
14. M. Bertolotti, S. Lagomarsino, F. Scudieri and D. Sette, *J. Phys.*, C **6**, L 177 (1973).
15. S. Kai, N. Yoshitsune and K. Hirakawa, *J. Phys. Soc. Jpn.*, **40**, 267 (1976).
16. L. M. Blinov, *J. Phys.* (Paris), **40**, C3-247 (1979).
17. J. S. Barley, E. Gelerinter and S. I. Ben-Abraham, *Mol. Cryst. Liq. Cryst.*, **87**, 251 (1982).
18. B. Jerome, *Rep. Prog. Phys.*, **54**, 391 (1991).
19. A. Saupe, *Mol. Cryst. Liq. Cryst.*, **21**, 211 (1973).
20. K. T. Schell and R. S. Porter, *Mol. Cryst. Liq. Cryst.*, **174**, 141 (1989).